

# Turbulence and Bifurcation in the Motion of an Hydrocyclone

Maria Morandi Cecchi<sup>(1)</sup> and Luca Salasnich<sup>(1)(2)</sup>

<sup>(1)</sup> Dipartimento di Matematica Pura ed Applicata, Università di Padova,  
Via Belzoni 7, I-35131 Padova, Italy

<sup>(2)</sup> Istituto Nazionale per la Fisica della Materia, Unità di Milano,  
Via Celoria 16, I-20133 Milano, Italy

## 1 The Hydrocyclone

The hydrocyclone is a tool used in different fields but mostly in mining industries to separate minerals. The minerals are put in a liquid or in a stable suspension of a chosen density which must be less than the density of the heavier minerals and greater than that of the lighter minerals [1,2,3].

Nowadays there is a strong interest for such tools, mostly in the processes where is possible to eliminate or reduce a lot the operation of grinding. This allows to reduce the cost of production and simplify the separation of minerals [4,5,6,7]. The modes of separation are two. One is the *static mode*, where the basis of the separation process is the gravitational force. The other is the *dynamic mode*, which operates by using a centrifugal force.

The static mode can be applied when is valid the relation  $F_g > F_D$ , where  $F_g$  is the gravitational force and  $F_D$  is the resistance force to the motion of mineral particles into the dense fluid. The relation is strictly related to the mass and dimension of the particles. As a consequence, the static separation can be used only with dimensions of the particles greater than 4–6 mm. Instead the dynamic separation can be used with a dimension of the particles less than 0.2–0.3 mm.

The hydrocyclone can be classified as:

- i) conic hydrocyclone (DMS);
- ii) cylindric hydrocyclone (DWP);
- iii) multi-stage hydrocyclone (TRI-FLOW).

The conic hydrocyclone is a cylinder connected in the lower part with a truncated cone of an angle between  $15^{\circ}$ – $20^{\circ}$ . The discharge of materials with less density (overflow) is done through a tube, the so-called *vortex finder*, with center in the upper cylinder. The discharge of the heavier materials (underflow) is realized through a tube (*apex*) which is connected to the lower base of the reversed conical section. The principle of functioning is equal in all systems. The material suspended in a dense fluid (made of the heavy material mixed to water) is introduced as the tangent through the inlet, producing into the hydrocyclone a vortical movement.

Under the effect of centrifugal forces the more heavy mineral particles put into the dense means will try to go to the wall of the hydrocyclone. In the central part along the central axis, the vortex gives the origin to a strong depression that allows the presence of a central nucleus (air core). These particles will travel along spiral trajectories and will leave the separator through the apex (under the effect of gravitational forces) that is in the lower part. Instead, the lighter particles, following the most part of the fluid, will tend to go in the direction of the central part, always following a spiral trajectory where by means of a strong ascensional kinetic field (due to a convenient difference of pressure applied to the two exits) will leave the hydrocyclone through the vortex finder put in the upper part.

For the cylindrical hydrocyclone and for the multi-stage hydrocyclone there is a tangential input of the dense means to originate a vortex and a central depression where an air core is situated. There will be a discharge in the lower part. The particles that are lighter will leave by a spiral trajectory through the vortex finder. The heavier particles will leave after going in the direction of the walls through the upper discharge (sink).

## 2 Confined swirling

Because of the effect of the walls the flow in a hydrocyclone is the result of a movement of confined swirling (vortex) and recirculating flow, which are generated by the difference of the means. There are many applications of the movement with vortex: not only the solid–liquid separation considered here but also solid–gas, gas–liquid and gas–gas separation as in combustion, production of jet, stabilization of fluxes in a plasma, heat exchange, valves and turbomachines [8].

The flux with vortex is the result of increasing the speed of the tangential component  $v_t$  by using a tool called *vortex generator*. Vortices having enough force can produce in the inner part of the fluid mass some fluxes in the opposite direction of the vortex. The configuration of this recirculation zone can depend on many different factors as the distribution of velocity, the geometrical shape of the place where the vortex is developed, etc.

A certain number of properties characterize the movement with confined vortex:

- a) the movement is 3-dimensional;
- b) the tangential component  $v_t$  of the velocity is predominant in the flux with the exception of the central turbulent part near the axis of the vortex;
- c) the radial component  $v_r$  of the velocity is very small;
- d) the predominant component of the axial velocity  $v_z$  is concentrated in a region close to the wall, having, close to the center, a component of inverse flux;
- e) the axis of symmetry can become a spiral with a dynamical behaviour in time;
- f) the microscopic flux is not very much related to the changes of velocity of the material into the system;
- g) the turbulence is always very great because the flux with vortex is in a system of stationary type.

### 3 Properties of vortex movement

Three are the properties that is necessary to introduce:

- 1) the Rankine profile for the tangential vorticity;
- 2) the vortex breakdown;
- 3) processing of vortex core.

As vortex of Rankine is intended the forced flux that can be interpreted as the combination of the rotation of a rigid body with contemporary presence of a free vortex where the action of the viscosity can be neglected. The rotation of the rigid body is classified as a rotational flux, instead the free vortex is classified as an irrotational flux. The zone where we have rotation of the rigid body is the central viscous region of the vortex and it is called nucleus of the vortex and also viscous nucleus. For a determined value of the axial coordinate such that the value taken by the tangential velocity is zero

such position is the center of the vortex which usually is different from the center of the place where the vortex develops [9,10,11].

To be able to deduce the characterized value of the Rankine vortex, one can follow the analysis prepared by Milne Thompson (1966). To such goal a plane flux is considered with a forced vortex of circular radius  $r_b$  and constant vorticity  $\zeta = \nabla \wedge v$  externally limited by an irrotational vortex.

By cylindrical coordinates and avoiding the axial and azimuthal variation two circular trajectories are considered around the forced vortex and with radius  $r_1 < r_b$  and  $r_b < r_2$  indicating by  $v_{\phi_1}$  and  $v_{\phi_2}$  the tangential velocity of the fluid in correspondence to the two limit trajectories.

Applying the Stokes theorem to the flux of the vector  $\zeta = \nabla \wedge v$  through the circular surfaces of ray  $r_1$  and  $r_2$  one obtains:

$$\int_{S_i} (\nabla \wedge v) \cdot ndS_i = \oint_{C_i} v dC_i \quad i = 1, 2 \quad (1)$$

where  $n$  indicates the versor of the normal to the generic surface  $dS_i$  and  $dC_i$  indicates an infinitesimal portion of the trajectory  $C_i$  of length  $2\pi r_i$ . By the development of these formulas one obtains the circulations  $\Gamma_1$  and  $\Gamma_2$

$$\Gamma_i = (\nabla \wedge v) \pi r_i^2 = 2\pi r_i v_{\phi_i}, \quad i = 1, 2 \quad (2)$$

from which it is possible to obtain the tangential velocity for the Rankine vortex

$$v_{\phi_i} = \frac{\Gamma_i}{2\pi r_i} = \frac{1}{2}(\nabla \wedge v)r_i, \quad i = 1, 2 \quad (3)$$

Remembering that the movement is realized into the plane  $(r, \phi)$  the relation  $2\omega = \nabla \wedge v$  applied to the direction  $z$  gives

$$v_{\phi_1} = \frac{\Gamma_1}{2\pi r_1} = \omega r_1, \quad (4)$$

$$v_{\phi_2} = \frac{\Gamma_2}{2\pi r_2} = \omega \frac{r_b^2}{r_2}. \quad (5)$$

Therefore the forced vortex is equivalent to a rotation of a rigid body with angular velocity  $\omega$ . The tangential velocity  $v_{\phi}(r)$  represents in the cartesian plane a line through the origin and of angular coefficient  $\omega$  with  $k_1 = \omega$  and  $k_2 = \omega r_b^2$ . The tangential velocity for forced vortex becomes  $v_{\phi_1} = \frac{\Gamma_1}{2\pi r_1} = k_1 r_1$  and for the free vortex  $v_{\phi_2} = \frac{\Gamma_2}{2\pi r_2} = k_2 / r_2$ .

## 4 Break of the vortex

If the tangential component of the velocity, namely of the Reynolds number, produces a zone of centered recirculation which signs the transition from a condition of flux with vortex that is said to be the break of the vortex and depend strongly from the swirl number  $S$ . This last one is a parameter that indicates the measure of the tangential velocity at the input. For two cylinders of ray  $R_1$  and  $R_2$  respectively that delimitate the zone of vorticity one has a  $S$  with the following expression

$$S = \frac{\int_{R_1}^{R_2} \rho r^2 v_z v_r dr}{R_2 \int_{R_1}^{R_2} \rho r v_z^2 dr} . \quad (6)$$

Sarbkaya, Escudier and Zehuder have studied the problem of break of the vortex. All these studies make a relation between the Reynolds number and the circulation number  $S$ .

## 5 Precession of the nucleus of the vortex

The recirculation zone generated by the break of the vortex is made by a jet with vortex in the strait direction and by the zone of inverse flux. These two quantities have distinct values for the axial and angular fluxes, sufficiently stable then exists an intermediate zone with great turbulence and fluctuations. This fluctuation originates the precession of the nucleus of forced vortex that tends to instability and moves around its symmetry axis. The different modes of precession of the nucleus and different stabilities are generally characterized using the Rayleigh number for the rotating fluid. This criteria says that a flux is stable if the quantity

$$\theta = \rho v_\phi r \quad (7)$$

grows with  $r$  (forced vortex) and this quantity is stable if it is constant with  $r$  (free vortex) and unstable if it decreases with  $r$ .

## 6 The nucleus of air

If the energy of a movement with vortex is big enough one has the generation along the rotation axis of the fluid of a nucleus of air, where the transversal

dimension depends directly on the pressure applied to the system and the form of such nucleus is cylindrical only in few cases. As it was said before, the axis of rotation does not coincide with the geometrical axis of the hydrocyclone. Namely for the nucleus of air there is no axial symmetry. Through the surface of the nucleus of air that is a liquid–air interphase there is a discontinuity of the gradient of the radial pressure due to the presence of two fluids with different density. The generation of the nucleus of air is due to the lowering of the pressure along the center of the vortex, to simplify the fluid is considered non viscous as was done by Milne Thompson. Considering a Rankine vortex one can indicate with  $p_1$  and  $p_2$  respectively the pressure into the vortex region, the pressure  $p_1$  with the formula

$$p_1 = \frac{1}{2}\rho\omega^2 r^2 + p_0, \quad (8)$$

and for the potential vortex the application of Bernulli theorem gives

$$\frac{p_2}{\rho} + \frac{1}{2}v_0^2 = \frac{p_\infty}{\rho}, \quad (9)$$

where  $v_\phi = 0$   $p = p_\infty$  when  $r$  goes to infinity. If the pressures are equal on the surface  $r = r_b$  one obtains for  $p_0$

$$p_0 = p_\infty - \rho\omega^2 r_b^2, \quad (10)$$

$$p_1 = p_\infty - \rho\omega^2 r_b^2 \left(1 - \frac{r^2}{2r_b^2}\right), \quad (11)$$

$$p_2 = p_\infty - \frac{1}{2}\rho\omega^2 \frac{r_b^2}{r^2}, \quad (12)$$

dividing by  $p_\infty$  the last expression and introducing the quantity

$$A = \rho\omega^2 \frac{r_b^2}{r_\infty^2}, \quad (13)$$

one obtains

$$\frac{p_1}{p_0} = 1 - A \left(1 - \frac{1}{2} \frac{r^2}{r_b^2}\right), \quad (14)$$

$$\frac{p_2}{p_0} = 1 - \frac{1}{2} A \frac{r^2}{r_b^2}. \quad (15)$$

The variation of the pressure in the two regions of the Rankine vortex gives a function of the quantity  $r/r_0$  and a behaviour of parabolic type given by

$$\frac{p_1}{p_\infty} - (1 - A) = \frac{1}{2}A \frac{r^2}{r_b^2}, \quad (16)$$

$$\left(\frac{p_2}{p_\infty} - 1\right) \frac{r^2}{r_0^2} = \frac{1}{2}A. \quad (17)$$

Different formulas have been given for the radius of the nucleus of air, the most important is that given by Concha and Barientos as

$$R_a = \frac{\sigma}{2\mu\alpha - \Delta p_a}, \quad (18)$$

where  $\alpha$  and  $\Delta p$  depend on the geometrical parameters and  $\mu$  is the viscosity of the fluid,  $\sigma$  the superficial tension,  $\alpha$  the radial component of the gradient of velocity evaluated in relation with  $R_a$ .  $\Delta p$  is the difference of pressure through the interphase air–liquid.

## 7 The dynamical model

The model of the Hydrocyclone is 3–dimensional, when to the sink and to the vortex finder a difference in the pressure is applied one has the generation of the air core where it is stable. The equations are the Navier–Stokes for the conservation of the mass and of the momentum [8]. We use the finite element method (FEM) [12] and the  $k$ – $\epsilon$  model [13], indicating by  $(u_i, p, T, c, k, \epsilon)$  all the variables and taking into account that the  $(k, \epsilon)$  turbulence model the field, this is characterized in terms of two variables using the turbulent energy  $k$  which is defined as

$$k = \frac{1}{2}u_i \cdot u_j, \quad (19)$$

$$\epsilon = \nu u_i \cdot u_j. \quad (20)$$

In the following we will use repeated indices to indicate summation and the symbol  $a_{,j}$  means  $\frac{\partial a}{\partial x_j}$ . Typical turbulent eddy velocity and length scales (denoted by  $u_i$  and  $l_i$ ) can be characterized as  $\sqrt{k}$  and  $k^{1.5}/\epsilon$ .  $\mu_t = \rho_0 c_\mu k/\epsilon^2$  is the turbulent viscosity and is directly related to the turbulent quantities  $k$  and  $\epsilon$ . A transport equation for  $k$  can be obtained from the Navier–Stokes

equations by a sequence of algebraic manipulations. This transport equation contains a number of unknown correlations. A second transport equation for  $\epsilon$  can also be derived from the Navier–Stokes equations. Application of a number of modeling assumptions simplifies these two equations to the well known equations of turbulent kinetic energy and viscous dissipation of the  $k$ – $\epsilon$  model. Then the unknown variables become  $(u_i, p, T, c, k, \epsilon)$  and the corresponding field equations are:

$$u_{j,j} = 0 , \quad (21)$$

$$\rho_0 \left( \frac{\partial u_i}{\partial t} + u_j u_{i,j} \right) = -p_{,i} + \rho_0 f_i - \rho_0 g_i [\beta_T (T - T_0) - \beta_c c] + [\mu (u_{i,j} + u_{j,i})_{,j}] , \quad (22)$$

$$\rho_0 c_p \left( \frac{\partial T}{\partial t} + u_j T_{,j} \right) = (\lambda T_{,j})_{,j} + \mu \Phi + H , \quad (23)$$

$$\rho_0 \left( \frac{\partial c}{\partial t} + u_j c_{,j} \right) = \rho_0 (\alpha c_{,j})_{,j} + q_c + R , \quad (24)$$

$$\rho_0 \left( \frac{\partial k}{\partial t} + u_j k_{,j} \right) = \left( \mu_0 + \frac{\mu_t}{\sigma_k} k_{,j} \right)_{,j} + \mu_t \Phi + \mu_t g_i \left( \frac{\beta_t}{\sigma_t} T_{,j} + \frac{\beta_c}{S_t} c_{,j} \right) - \rho_0 \epsilon , \quad (25)$$

$$\rho_0 \left( \frac{\partial \epsilon}{\partial t} + u_j \epsilon_{,j} \right) = \left( \mu_0 + \frac{\mu_t}{\sigma_\epsilon} \epsilon_{,j} \right)_{,j} + c_1 \frac{\epsilon}{k} \mu_t \Phi + c_1 (1 - c_3) \frac{\epsilon}{k} g_j \left( \frac{\mu_t}{\sigma_t} \beta_T T_{,j} + \frac{\mu_t}{S_t} \beta_c c_{,j} \right) - \rho_0 c_2 \frac{\epsilon^2}{k} , \quad (26)$$

where  $\Phi = 2\epsilon_{ij}\epsilon_{ij}$ , with  $\epsilon_{ij} = \frac{1}{2}(u_{i,j} + u_{j,i})$  the strain stress tensor.  $\alpha$  is the slip coefficient,  $\beta_T$  and  $\beta_c$  are the volume expansion coefficients,  $\lambda$  is the thermal conductivity,  $g_i$  is the gravitational force vector. After years of testing the  $k$ – $\epsilon$  model, the choice of the quantity taken as empirical constants has led to the following recommended set of model constants:  $c_\mu = 0.09$ ,  $\sigma_k = 1.00$ ,  $\sigma_\epsilon = 1.30$ ,  $\sigma_\tau = 0.9$ ,  $S_t = 0.9$ ,  $c_1 = 1.44$ ,  $c_2 = 1.92$ ,  $c_3 = 0.8$ .

## 8 Turbulence Modelling

The system of equations (21–26) is discretized by the usual finite element method. It is important to note that the introduction of the eddy viscosity concept makes the total effective viscosity a function of position, thus necessitating a stress divergence formulation. Using the approximation

$$k(x, t) = \phi^T K(t) , \quad (27)$$

$$\epsilon(x, t) = \phi^T E(t) . \quad (28)$$

Within each element, the velocity, pressure and temperature field are approximated by

$$u_i(x, t) = \phi^T U_i(t) , \quad (29)$$

$$p(x, t) = \psi^T P(t) , \quad (30)$$

$$T(x, t) = \theta^T T(t) . \quad (31)$$

where  $U_i$ ,  $P$  and  $T$  are column vectors of element nodal point unknowns and  $\phi$ ,  $\psi$  and  $\theta$  are column vectors of the interpolation functions. Herein the same basis functions are employed but cost-effective restrictions. Substitution of these approximations into the field equations and boundary conditions yields a set of equations:

$$f_1(\phi, \psi, \theta, U_i, P, T) = R_1 , \quad (32)$$

$$f_2(\phi, U_i) = R_2 , \quad (33)$$

$$f_3(\phi, \theta, U_i, T) = R_3 , \quad (34)$$

where  $R_1$ ,  $R_2$ , and  $R_3$  are the residuals (errors) resulting from the use of the approximations of equation (3). The process results in the following finite system of nonlinear ordinary differential equations:

$$\begin{aligned} & \begin{pmatrix} M & 0 & 0 & 0 & 0 & 0 & 0 \\ 0 & M & 0 & 0 & 0 & 0 & 0 \\ 0 & 0 & M & 0 & 0 & 0 & 0 \\ 0 & 0 & 0 & N & 0 & 0 & 0 \\ 0 & 0 & 0 & 0 & 0 & 0 & 0 \\ 0 & 0 & 0 & 0 & 0 & M & 0 \\ 0 & 0 & 0 & 0 & 0 & 0 & M \end{pmatrix} \begin{pmatrix} \dot{U}_1 \\ \dot{U}_2 \\ \dot{U}_3 \\ \dot{T} \\ \dot{P} \\ \dot{K}_1 \\ \dot{E}_1 \end{pmatrix} + \\ & + \begin{pmatrix} K_{11} & K_{12} & K_{13} & K_{14} & -C_1 & 0 & 0 \\ K_{21} & K_{22} & K_{23} & K_{24} & -C_2 & 0 & 0 \\ K_{31} & K_{32} & K_{33} & K_{34} & -C_3 & 0 & 0 \\ 0 & 0 & 0 & K_{44} & 0 & 0 & 0 \\ -C_1^T & -C_2^T & -C_3^T & 0 & 0 & 0 & 0 \\ 0 & 0 & 0 & 0 & 0 & K_{66} & 0 \\ 0 & 0 & 0 & 0 & 0 & 0 & K_{77} \end{pmatrix} \begin{pmatrix} U_1 \\ U_2 \\ U_3 \\ T \\ P \\ K \\ E \end{pmatrix} = \begin{pmatrix} F_1 \\ F_2 \\ F_3 \\ F_4 \\ 0 \\ F_6 \\ F_7 \end{pmatrix} . \quad (35) \end{aligned}$$

The sub-matrices  $M$ ,  $N$  and  $C_i$  are given by

$$M = \int_V \rho_0 \phi \phi^T dV , \quad (36)$$

$$N = \int_V \rho_0 c_p \theta \theta^T dV , \quad (37)$$

$$C_i = \int \frac{\partial \phi}{\partial x_j} \psi^T dV . \quad (38)$$

The remaining sub-matrices take the following form for  $i, j = 1, 2, 3$ . Note that parentheses on repeated indices indicate a relaxation of the summation convention:

$$K_{(i)(i)} = \int_V \rho_0 u_j \phi \phi_{,j}^T dV + \int_V \mu (\phi_{,j} \phi_{,j}^T + \phi_{,(i)} \phi_{,(i)}^T) dV , \quad (39)$$

$$K_{ij} = \int_V \mu \phi_{,i} \phi_{,j}^T dV \quad i \neq j , \quad (40)$$

$$K_{i4} = \int_V \rho_0 \beta g_i \phi \phi^T dV , \quad (41)$$

$$K_{44} = \int_V \rho_0 c_p u_i \phi \phi_{,i}^T dV + \int_V \lambda \phi_{,j} \phi_{,j}^T dV , \quad (42)$$

$$K_{66} = \int_V \rho_0 u_j \phi \phi_{,j}^T dV + \int_V \frac{\mu_t}{\sigma_\epsilon} \phi_{,j} \phi_{,j}^T dV + \int_V \rho_0 \frac{\epsilon}{k} \phi \phi^T dV , \quad (43)$$

$$K_{77} = \int_V \rho_0 u_j \phi \phi_{,j}^T dV + \int_V \frac{\mu_t}{\sigma_\epsilon} \phi_{,j} \phi_{,j}^T dV + \int_V \rho c_2 \frac{\epsilon}{k} \phi \phi^T dV , \quad (44)$$

$$F_i = \int_V \rho f_i dV + \int_V \rho g_i (1 + \beta T_0) \phi dV , \quad (45)$$

$$F_4 = - \int_S \lambda \theta \frac{\partial T}{\partial n} dS + \int_V q_s \theta dV + \int_V \mu \Phi \theta dV , \quad (46)$$

$$F_6 = \int_S \frac{\mu_t}{\sigma_k} \frac{\partial k}{\partial n} \phi dS + \int_V \mu_t \Phi \phi dV , \quad (47)$$

$$F_7 = \int_S \frac{\mu_t}{\sigma_\epsilon} \frac{\partial \epsilon}{\partial n} \phi dS + \int_V c_1 \frac{\epsilon}{k} \mu_t \Phi \phi dV . \quad (48)$$

Each of the above integrals are evaluated using the isoparametric map/quadrature procedure. Then, using the isothermal hypothesis, the solution is obtained by applying the Galerkin Finite Element Method in the usual fashion. In Figures 1–3 we show our FEM numerical results, which are in good agreement with the experimental data [5,6,7]. See figure captions for further details.

## 9 A simple model for the Hydrocyclone

In this section we study a simple 3D family of maps which shows some of the properties of the Hydrocyclone.

We call  $(\rho, \theta, v_z)$ -polypous the family of planar maps  $f_{\rho\theta} : \mathbf{R}^3 \rightarrow \mathbf{R}^3$  such that  $f_{\rho\theta v_z}(x, y, z) = (f_{\rho\theta v_z}^{(1)}(x, y, z), f_{\rho\theta v_z}^{(2)}(x, y, z), f_{\rho\theta v_z}^{(3)}(x, y, z))$ , with  $\rho \geq 0$ ,  $\theta \in [-2\pi, 2\pi]$ ,  $v_z \in \mathbf{R}$  and:

$$\begin{aligned} f_{\rho\theta v_z}^{(1)}(x, y, z) &= x \rho \cos \theta + y \rho \sin \theta - \frac{x^3}{3} - \frac{y^3}{3}, \\ f_{\rho\theta v_z}^{(2)}(x, y, z) &= -x \rho \sin \theta + y \rho \cos \theta + \frac{x^3}{3} - \frac{y^3}{3}, \\ f_{\rho\theta v_z}^{(3)}(x, y, z) &= z + v_z. \end{aligned} \quad (49)$$

In Figure 4 and 5 we show the dynamics of our map for  $\rho = 1$ ,  $v_z = -1$  and three different values of the  $\theta$  parameter. The trajectories follow a spiral and tend to go down in the direction of the central part. By taking a positive value for the velocity  $v_z$  and different values for the parameter  $\theta$  we can model also the trajectories of particles which go in the upper part.

Because the dynamics of the  $(\rho, \theta, v_z)$ -polypous in the  $z$  direction is trivial, we analyze in detail the  $(\rho, \theta, v_z)$ -polypous on the  $(x, y)$  plane for  $v_z = 0$  (see also [14]).

To characterize the  $(\rho, \theta)$ -polypous we can calculate the Jacobian

$$Df_{\rho\theta}(x, y) = \begin{pmatrix} \rho \cos \theta - x^2 & \rho \sin \theta - y^2 \\ -\rho \sin \theta + x^2 & \rho \cos \theta - y^2 \end{pmatrix}. \quad (50)$$

The trace of  $Df_{\rho\theta}$  is given by

$$Tr(Df_{\rho\theta}(x, y)) = 2\rho \cos \theta - (x^2 + y^2), \quad (51)$$

and the determinant

$$\det(Df_{\rho\theta}(x, y)) = 2x^2y^2 - \rho(\cos \theta + \sin \theta)(x^2 + y^2) + \rho^2. \quad (52)$$

A direct calculus shows that the eigenvalues of the  $\rho\theta$ -polypous are given by

$$\lambda_{1,2}(x, y) = \frac{1}{2} [Tr(Df_{\rho\theta}(x, y)) \mp \sqrt{Tr(Df_{\rho\theta}(x, y))^2 - 4\det(Df_{\rho\theta}(x, y))}]. \quad (53)$$

The  $(\rho, \theta)$ -polypous has a fixed point in  $(0, 0) \in \mathbf{R}^2$ . This fixed point is hyperbolic if  $\rho \neq 1$ . It is asymptotically stable, i.e an attractor, if  $\rho < 1$  and it is unstable if  $\rho > 1$ . The  $(\rho, \theta)$ -polypous is differentiable but it is not a homeomorphism because it is not invertible: there are several anti-images of the origin, one of them is obviously the origin itself.

Now we discuss in great details the very interesting case  $\rho = 1$ : The  $(\rho, \theta)$ -polypous has a non-hyperbolic fixed point in  $(0, 0) \in \mathbf{R}^2$  if  $\rho = 1$ . This fixed point is asymptotically stable if  $\theta \in ]-\pi/4, 3\pi/4[$ , but  $\theta \neq 0$ . First we observe that when  $\theta = 0$  and  $\theta = \pi$  the eigenvalues of  $Df_{1\theta}(0, 0)$  are real numbers. For all the other values of  $\theta$  the eigenvalues are complex but not real and have unitary modulus.

We call  $d_\theta(x, y) = \det(Df_{1\theta}(x, y))$  and obtain

$$\begin{aligned} \nabla d_\theta(x, y) &= (4xy^2 - 2(\cos \theta + \sin \theta)x, 4x^2y - 2(\cos \theta + \sin \theta)y), \\ Hd_\theta(x, y) &= \begin{pmatrix} 4y^2 - 2(\cos \theta + \sin \theta) & 8xy \\ 8xy & 4x^2 - 2(\cos \theta + \sin \theta) \end{pmatrix}, \end{aligned}$$

and its eigenvalues in  $(0, 0)$  are equal to  $-2(\cos \theta + \sin \theta)$ . The Hessian  $Hd_\theta(0, 0)$  is negative definite if  $(\cos \theta + \sin \theta) > 0$ , thus if  $\theta \in ]-\pi/4, 3\pi/4[$ . For these values of  $\theta$  the origin is a local maximum and by using the theorem of reference [14] ( $\theta \neq 0$ ) we have that  $(0, 0)$  is asymptotically stable.

Consider  $\theta = 2\pi/n$ ,  $n \geq 3$ . The dynamics of  $f_{1\theta}$  is attractive and, because  $Df_{1\theta}(0, 0)$  is a rotation of  $\theta$ , it looks like a polypous with  $n$  branches.

Moreover, if we add to the first two components of the  $(\rho, \theta, v_z)$ -polypous an oscillatory term  $\cos(\omega z)$  we can get an elicoidal cylinder superimposed to the spiral dynamics (see Figure 6). So the modified  $(\rho, \theta, v_z)$ -polypous give rise also to the elicoidal effect, which has been recently observed experimentally [7].

## 10 Conclusions

In this paper we have studied the turbulence and bifurcation in the motion of an Hydrocyclone by using a Finite Element Method based on the Navier-Stokes equations. The numerical results are in good agreement with the experimental data. We have also analyzed a simple 3D family of maps which

models very well the behaviour of the trajectories of the light and heavy particles in the Hydrocyclone.

## References

- [1] J.L. Smith, "An analysis of the vortex flow in the cyclone separator", Jour. of Basic Engineering–Trans. of ASME, 609 (1962).
- [2] D. Bradley, *The hydrocyclones* (Pergamon, London, 1965).
- [3] J. Mizrahi and E. Cohen, "Studies of some factor influencing the action of hydrocyclones", Trans. Instr. Min. Metall. **75**, C318 (1966).
- [4] M.I.G. Bloor and D.B. Ingham, "The flow in industrial cyclones", Jour. of Fluid Mechanics, **178**, 507 (1987).
- [5] A. Barrientos, R. Sampaio and F. Concha, "Effect of air core on the preformation of a Hydrocyclone", in Proceedings XVIII International Mineral Processing Congress, May 1993, Sidney, pp. 267–270.
- [6] F. Concha, A. Barrientos, J. Montero and R. Sampaio, "Air core and roping in hydrocyclones", Symposium on Comminution 1994, Stockholm, pp. 814–823.
- [7] B. Chine, F. Concha and A. Barrientos, "A finite difference solution of the swirling flow in a hydrocyclone", in Proc. of International Conference on Finite Elements in Fluids – New Trends and Applications, Venezia, 15–21 October, 1995.
- [8] G.K. Batchelor, *An introduction to fluid dynamics* (Cambridge University Press, Cambridge, 1967).
- [9] S.V. Patankar and D.B. Spalding, "A calculation procedure for heat, mass and momentum transfer in three-dimensional parabolic flows", Int. Jour. of Heat and Mass Transfer, **15**, 1787 (1972).
- [10] S.V. Patankar, *Numerical heat transfer and fluid flow* (Hemisphere Publ. Corp., New York, 1980).

- [11] K.T. Hsieh and K. Rajamani, "Mathematical model of the hydrocyclone based on physics of fluid flow" *AIChE Jour.* **37**, 735 (1991).
- [12] G.F. Carey and J.T. Oden, *Finite Elements: Fluid Mechanics* (Prentice-Hall, New Jersey, 1986).
- [13] Fluid Dynamics Analysis Package, FIDAP 7.0, Fluid Dynamics International, Inc. (1993).
- [14] M. Morandi Cecchi and L. Salasnich, "Non-hyperbolic dynamics: a family of special functions", *Open System and Information Dynamics*, vol. 5 (1998).

## Figure Captions

**Figure 1:** FEM trajectories of heavy particles in the Hydrocyclone.

**Figure 2:** FEM trajectories of light particles in the Hydrocyclone.

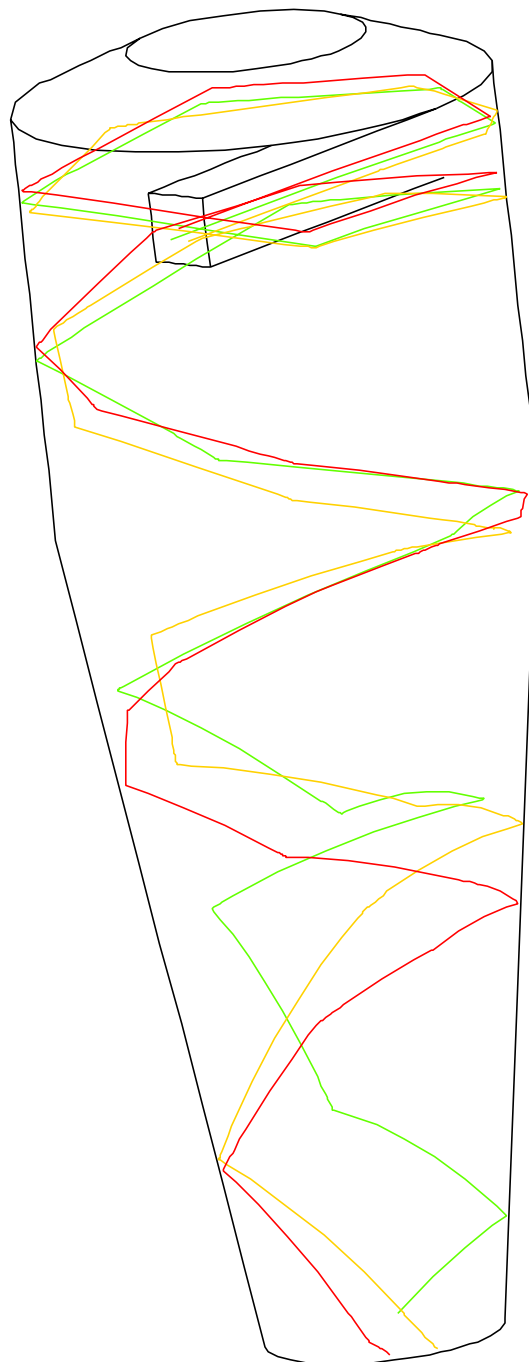
**Figure 3:** FEM velocity field in the  $z$  direction for the Hydrocyclone.

**Figure 4:** Spiral trajectories obtained with the  $(1, \theta, -1)$ -polypous in the  $(x, y)$  plane. 1)  $\theta = 0.1 \cdot \pi$ , 2)  $\theta = 0.03 \cdot \pi$ , 3)  $\theta = 0.05 \cdot \pi$ .

**Figure 5:** Same trajectories of Figure 4 in 3D.

**Figure 6:** Elicoidal cylinder obtained with the modified  $(1, 0.2 \cdot \pi, -1)$ -polypous with  $\omega = 0.2$ .

# Heavy particles



PARTICLE  
PATH PLOT

PARTICLE PATH

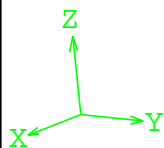
FROM TIME:  
.0000E+00

TO TIME:  
.1330E+03

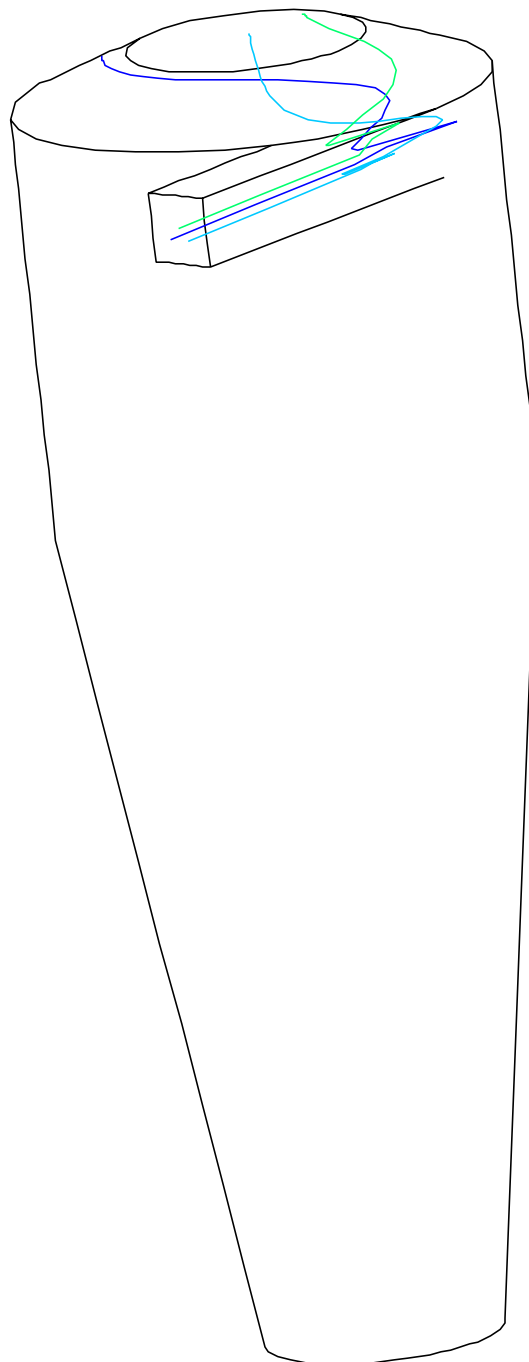
VIEW DIRECTION

VX .100E+01  
VY .887E+00  
VZ .325E+00  
ANG .614E+01

FIDAP 7.51  
20 Sep 96  
14:50:32



Light particles



PARTICLE  
PATH PLOT

PARTICLE PATH

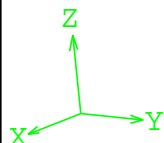
FROM TIME:  
.0000E+00

TO TIME:  
.1838E+02

VIEW DIRECTION

VX .100E+01  
VY .887E+00  
VZ .325E+00  
ANG .614E+01

FIDAP 7.51  
20 Sep 96  
14:37:02



Z COMP. VELOC.  
CONTOUR PLOT

LEGEND

-- -.7319E-01  
-- -.5606E-01  
-- -.3892E-01  
-- -.2178E-01  
-- -.4648E-02  
-- .1249E-01  
-- .2962E-01  
-- .4676E-01  
-- .6390E-01  
-- .8103E-01

MINIMUM  
-.19373E+00  
MAXIMUM  
.10854E+00

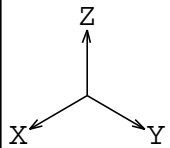
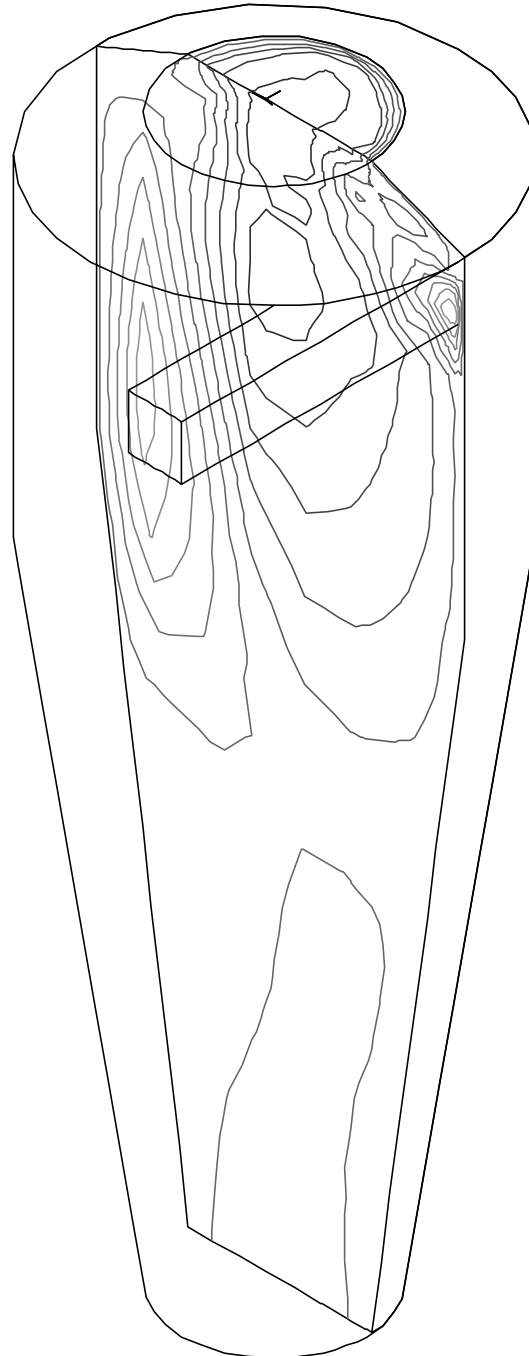
PLANE COEFF.S

A .100E+01  
B .000E+00  
C .000E+00  
D .619E-01

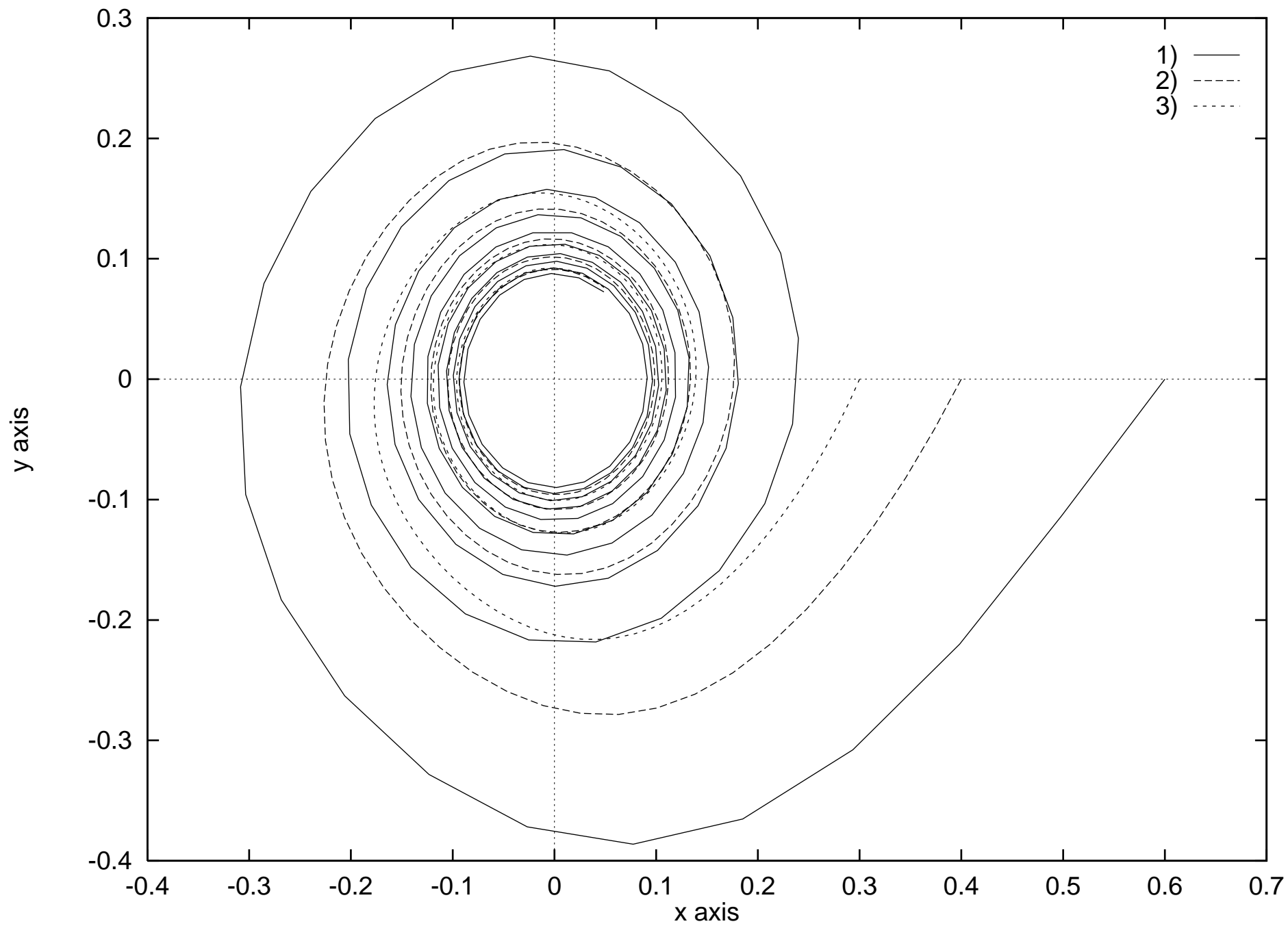
VIEW DIRECTION

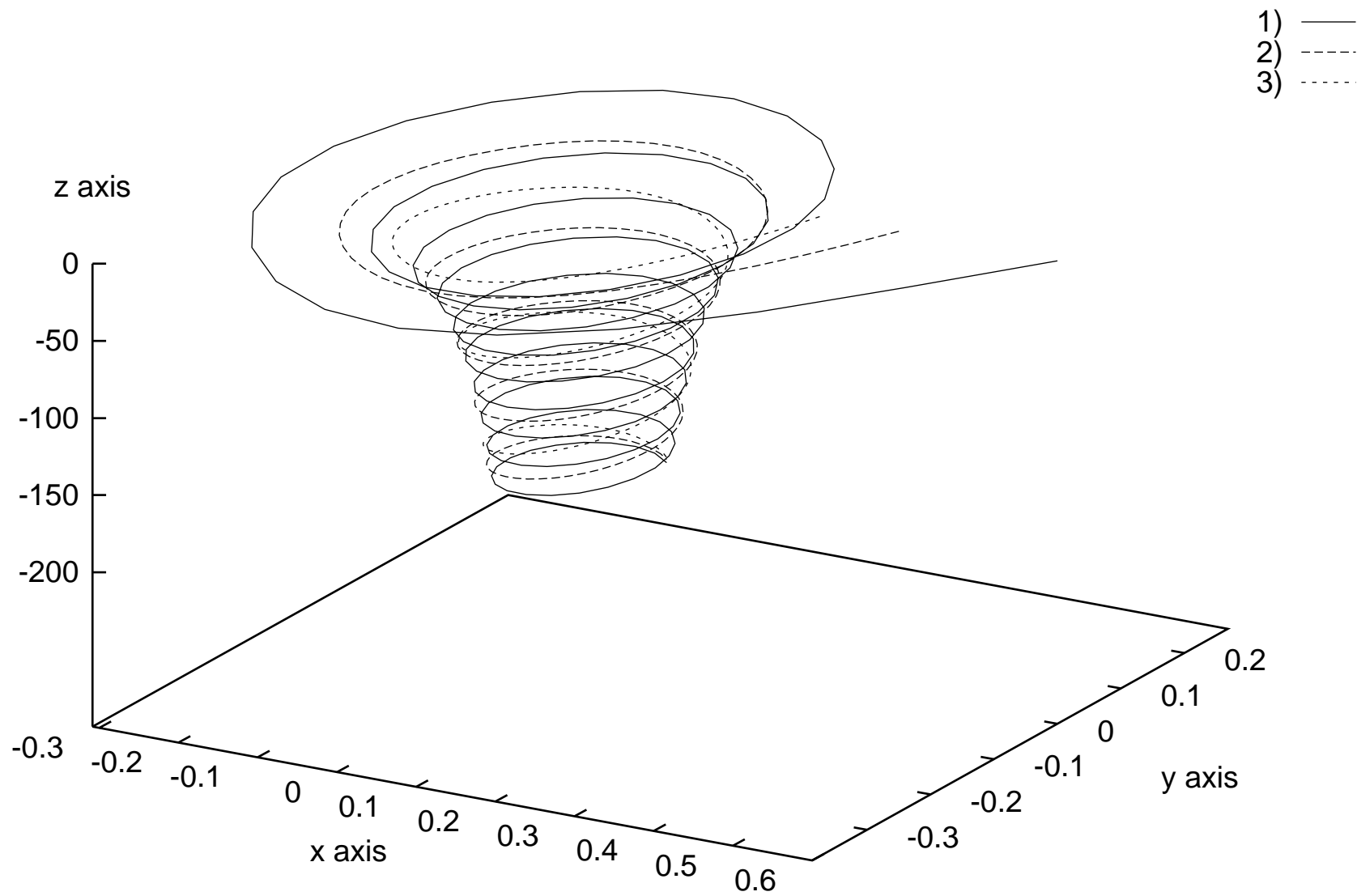
VX .100E+01  
VY .100E+01  
VZ .100E+01  
ANG .000E+00

FIDAP 7.51  
10 Mar 98  
12:04:09









4) —

